Steam Reforming of Ethanol over Skeletal Ni-based Catalysts: A Temperature Programmed Desorption and Kinetic Study

Chengxi Zhang, Shuirong Li, Gaowei Wu, Zhiqi Huang, Zhiping Han, Tuo Wang, and Jinlong Gong
Key Laboratory for Green Chemical Technology of Ministry of Education, School of Chemical Engineering and Technology, Tianjin University, Collaborative Innovation Center of Chemical Science and Engineering, Tianjin 300072, China

DOI 10.1002/aic.14264
Published online November 20, 2013 in Wiley Online Library (wileyonlinelibrary.com)

An investigation on reaction scheme and kinetics for ethanol steam reforming on skeletal nickel catalysts is described. Catalytic activity of skeletal nickel catalyst for low-temperature steam reforming has been studied in detail, and the reasons for its high reactivity for H_2 production are attained by probe reactions. Higher activity of water gas shift reaction and methanation contributes to the low CO selectivity. Cu and Pt addition can promote WGSR and suppress methanation, and, thus, improve H_2 production. A reaction scheme on skeletal nickel catalyst has been proposed through temperature programmed reaction spectroscopy experiments. An Eley-Rideal model is put forward for kinetic studies, which contains three surface reactions: ethanol decomposition, water gas shift reaction, and methane steam reforming reaction. The kinetics was studied at 300–400°C using a randomized algorithms method and a least-squares method to solve the differential equations and fit the experimental data; the goodness of fit obtained with this model is above 0.95. The activation energies for the ethanol decomposition, methane steam reforming, and water gas shift reaction are 187.7 kJ/mol, 138.5 kJ/mol and 52.8 kJ/mol, respectively. Thus, ethanol decomposition was determined to be the rate determining reaction of ethanol steam reforming on skeletal nickel catalysts. © 2013 American Institute of Chemical Engineers *AIChE J*, 60: 635–644, 2014

Keywords: ethanol steam reforming, Raney ni, kinetics, eley-rideal mechanism, ethanol decomposition

Introduction

Currently most of the energy we use comes from fossil fuels, and particularly, the utilization of fossil fuels has been surged in the 20th century. Thus, their reserves come at a time of diminishing,[1] and the emission of NO_x and SO_x from fossil fuels results in severe pollution of the environment.[2] The status encourages us to develop green and renewable energy framework, including hydrogen energy. Among a variety of production technologies of hydrogen, steam reforming is one of the most widely employed.[3,4] Bioethanol steam reforming for hydrogen production has become a research emphasis in energy and catalysis fields since bioethanol is cheap, easy to handle, low in toxicity, and thermodynamically feasible to decompose.[5] Nickel-based catalysts have been extensively used in ethanol steam reforming (ESR) due to its excellent ability in C—C, C—H, C—O bond cleavage and dehydrogenation.[6–11]

The specific surface area of active nickel species is important to obtain high-ethanol conversion and H_2 yield.[12–14] Skeletal nickel-based catalysts have been shown to have higher specific surface areas than conventional supported nickel catalysts, and they have superior activity in steam reforming reaction, even at low temperatures.[14] However, the role of the catalyst in controlling the selectivity to H_2 has not been thoroughly understood, and a kinetic study is necessary for scaling-up the process and guiding its operation. Several kinetic studies have been applied for supported metal nanocatalysts. Idem et al. has proposed a kinetic model on a 15% Ni/Al_2O_3 catalyst for the production of hydrogen from crude ethanol reforming, in which an Eley-Rideal (E-R) assumption was used and the rate-determining step (RDS) was the dissociation of adsorbed ethanol.[15] Llera et al. proposed a Langmuir-Hinshelwood (L—H) model using a nickel based catalyst in the temperature range of 873–923 K, which involving ethanol decomposition (ED), ESR, methane steam reforming (MSR), and water gas shift reaction (WGSR).[16] They used surface reactions of the above four reactions as RDSs. In Graschinsky's work, the reaction scheme of ESR on Rh supported catalysts also consists of the four surface reactions (ED, ESR, WGSR and MSR), in which the RDS is a reaction between two adsorbed species, and a Langmuir Hinshelwood (L—H) model was used to fit the experimental data.[17] Ciambelli et al. carried out a preliminary kinetic study for steam reforming of ethanol on Pt/CeO_2 using power law model and proposed that the main promoted reactions were ED, MSR, and WGSR.[18] Temperature programmed desorption experiments were also employed to suggest a surface reaction mechanism involving the following step (1) ethanol dissociative adsorption on

Correspondence concerning this article should be addressed to at jlgong@tju.edu.cn.

catalyst surface to form acetaldehyde intermediate, (2) decarbonylation to produce mainly H_2, CH_4 and CO, and (3)WGSR of CO adsorbed on Pt sites to produce H_2 and CO_2. Additionally, Laborde et al. proposed a general kinetic model for ESR based on a L—H mechanism which was valid for a wide range of water/ethanol feed ratios and temperatures.[19] These kinetic investigations on a nickel-based catalyst have been proved to be useful in the design of ethanol steam reformer. It can be seen that power-law model, E-R model and L—H model kinetic expressions are reported in the kinetic studies,[16–18,20,21] and the four surface reactions (ED, ESR, MSR, WGSR) have been typically considered in the reaction scheme as the RDSs.

It is a general consensus that ethanol adsorption on the active site is the first step,[15,22–24] although few others proposed that the ethanol simply decomposes at the active site without molecular adsorption.[21,25,26] Water activation can follow different routes. It could dissociatively adsorb on the surface to form OH and H,[21,27,28] or reacts with adsorbed species (e.g., CO) following the E-R mechanism.[15,29] Nevertheless, Ni surfaces or pure Ni catalysts have low probability to dissociate water due to the less defect sites to active water compared to supported catalysts.[30]

Indeed, the earlier kinetics and mechanisms were all investigated on supported catalysts, and the role of pure nickel on the distribution of products remained elusive. Therefore, this article describes a series of skeletal nickel-based catalysts for ESR,[14] which showed high reactivity compared to conventional supported catalysts in low-temperature steam reforming. The enhanced activity was believed to be ascribed to the increased active nickel surface areas. The aim of this work is to elucidate the products distribution and postulate a kinetic scheme from temperature programmed reaction spectroscopy (TPRS) experiment. WGSR and methanation probe reactions were also carried out to understand the origin of the elimination of CO in ESR. A kinetic model based on E-R assumptions was then built-up to fit the experimental data.

Experimental

Catalysts preparation

Preparation of the Skeletal Ni Catalysts. Under gentle stirring, 2 g of Ni-Al alloy powder (50 wt % Ni + 50 wt % Al, Shanghai Chemical Reagent Factory) was added to an aqueous solution of NaOH (120 mL, 20 wt %) at 323 K. The resultant mixture was stirred at 343 K for 3 h. The precipitate was sequentially washed with distilled water and ethanol, and stored in ethanol prior to the use.

Preparation of Alloyed Skeletal Ni Catalysts. A certain amount of $Cu(CH_3COO)_2$ (Tianjin Fuchen Chemical Reagent Factory, 99.5%), $Co(CH_3COO)_2$ (Tianjin Fuchen Chemical Reagent Factory, 99.5%) and $Pt(NO_3)_2$ (Guiyang platinum industry, Ltd.; Pt content, 5.7%) solution was added to the above skeletal Ni catalyst, respectively. The volume of solution was kept at 70 mL. The solution was stirred at 343 K for 1 h. The precipitate was washed with water until no ions were detected in the filtrate, and then it was washed with ethanol and stored in ethanol. Prior to activity test and characterization, all catalysts were dried at 80°C under vaccum for 5 h and were protected under the nitrogen ambient.

Preparation of Ni/SiO_2 catalyst. Commercial SiO_2 (Qingdao Yurui chemical Co., Ltd.) was calcined at 973 K for 2 h. Ni/SiO_2 was prepared by the incipient wetness impregnation method. SiO_2 was impregnated in a $Ni(NO_3)_2{\cdot}6H_2O$ ethanol solution (1 M) by mechanical agitation at 323 K for 12 h, followed by evaporated at 333 K using vacuum rotary until the ethanol was removed. The resultant solid was dried at 373 K for 12 h, and then calcined at 973 K for 2 h. The amount of Ni loading was fixed to 15 wt %.

Activity test

Ethanol Steam Reforming. Catalytic tests were conducted at atmospheric pressure in a quartz fixed-bed reactor loaded with 0.1 g catalyst mixed with 1 mL quartz particles. Prior to the test, the catalysts were reduced at 673 K *in situ* for 1 h in a flow of 10 vol % H_2/N_2 (50 mL/min). The liquid solution (0.033–0.26 mL/min) with a water/ethanol molar ratio of 8 (equals to steam to carbon ratio (S/C) = 4) was fed through an HPLC pump into a heated chamber (423 K) to evaporate the solution completely in the stream of N_2 (400 mL/min). The products were analyzed online by two gas chromatographs. One is equipped with a FID, and a Porapak-Q column with N_2 as a carrier gas to analyze the organic species such as ethanol and methane. The other one is equipped with a TCD and a TDX-01 column using He as a carrier gas to monitor the incondensable gas species including hydrogen, carbon dioxide, carbon monoxide and methane.

Probe Reactions. Catalytic activity of WGSR and methanation for all catalysts was evaluated in the same flow reactor at 623 K. Appropriate amounts of catalysts (25 mg, 60–80 mesh) were loaded between the two layers of quartz wool in the quartz tube reactor. Before the test, the catalysts were reduced at 673 K *in situ* for 1 h in a flow of 10 vol % H_2/N_2 (50 mL/min). For WGSR, water was fed at 0.032 mL/min through an HPLC pump into a heated chamber (423 K) to evaporate the water completely in the mix stream of N_2 (40 mL/min) and CO (20 mL/min). For methanation, CO (20 mL/min), H_2 (60 mL/min), and N_2 (20 mL/min) were fed after mixing thoroughly. The products were analyzed online by gas chromatographs equipped with a TCD and a TDX-01 column using He as a carrier gas.

Characterization

BET Experiment. Textual properties of the catalysts were measured using a Micromeritics Tristar 3000 analyzer by nitrogen adsorption at 77 K. The specific surface areas were calculated from the isotherms using the BET method, and the pore distribution and the cumulative volumes of pores were obtained by the BJH method from the desorption branches of the adsorption isotherms.

CO Pulse Chemisorption. CO adsorption capacity on Ni surfaces was determined by CO pulse chemisorption (Micromeritics AUTOCHEM II 2920). After the catalyst was reduced at 673 K for 1.0 h under 10% H_2/Ar flow, it was cooled down to room temperature under the He atmosphere, and then CO pulses were injected until the eluted peak area of consecutive pulses was constant. The CO/Ni atomic ratio (the amount of CO adsorbed divided by the amount of nickel atom in the catalyst) was calculated from the volume of CO adsorbed and the amount of nickel in the catalyst.

TPRS Experiment. TPRS experiment was carried out in a flow reactor (4 mm internal diameter) connected to a QIC 20 HIDEN quadrupole mass spectrometer. Prior to any measurements, all samples were reduced *in situ* using a flow of 10

Table 1. Physical Properties of Skeletal Ni based Catalysts

Sample	M/Ni (wt. %)[a]	BET surface area/(m^2/g)	Average pore diameter/(Å)	Pore volume/(cm^3/g)	Particle size/(nm)[b]	Crystal size/(nm)[c]	S_H/(m^2/g_{Ni})[d]
skeletal Ni	0.0	56.1	41.9	0.069	6.3 ± 1.5	5.1	14.2
Cu/skeletal Ni	1.7	52.6	43.1	0.076	6.6 ± 1.5	5.1	14.5
Co/skeletal Ni	1.2	51.1	44.2	0.073	5.4 ± 1.2	4.7	14.7
Pt/skeletal Ni	1.1	99.2	31.2	0.047	4.4 ± 1.4	4.8	14.9
Ni/SiO_2	n.a.	384.3	32.9	0.24	7.9 ± 1.3	7.5	6.3

[a]determined by ICP-OES.
[b]determined from TEM graph (statistics on 20 particles randomly picked up from TEM images).
[c]Ni crystal size determined by the Scherrer equation from the (111) plane of Ni in XRD patterns.
[d]active surface area determined by H_2 pulse chemisorption.

vol% H_2/Ar (30 mL/min). After purging with Ar for 15 min, the sample was cooled under Ar to room temperature (293 K). For adsorption/desorption of ethanol, a mixture containing 0.3% EtOH in Ar was directed through the catalyst bed at a rate of 30 mL/min for 30 min in order to saturate the catalyst surface with ethanol. Adsorption was followed by purging with Ar for 15 min. The temperature was subsequently ramped from 293 K to 1073 K with a linear rate of 10 K/min under Ar flow (30 mL/min). For adsorption/desorption of ethanol-water solution, a mixture containing 0.3% EtOH and 2.4% H_2O in Ar was directed through the catalyst bed at a rate of 30 mL/min for 30 min. Then Ar was purged for 15 min so as to clean all lines; after this treatment, temperature was ramped from 293 K to 1073 K with a linear rate of 10 K/min under Ar flow (30 mL/min). For temperature-programmed surface reaction, a mixture containing 0.3% EtOH and 2.4% H_2O in Ar was directed through the catalyst bed at a rate of 30 mL/min while temperature was ramped from 293 K to 1073 K with a linear rate of 10 K/min. The reactor effluent was continuously monitored by the mass spectrometer and gas-phase composition was calculated from the mass spectrometer signal at m/e ratios of 44, 40, 31, 28, 15, 2 for CO_2, Ar, C_2H_5OH, CO, CH_4, and H_2, respectively.

Conversion, selectivity and TOF calculations

$$X_{EtOH} = \frac{F_{EtOH,in} - F_{EtOH,out}}{F_{EtOH,in}} \times 100\%$$

$$S_{H_2}(\%) = \frac{(\text{moles of } H_2 \text{ produced})}{6 \times (\text{moles of ethanol converted})} \times 100$$

$$S_j(\%) = \frac{(\text{moles of } j \text{ produced}) \times i}{2 \times (\text{moles of ethanol converted})} \times 100$$

where j represents the carbon containing species in the products, including CO, CO_2 CH_4, C_2H_4, C_2H_6, CH_3CHO, and CH_3COCH_3. i is the number of carbon atoms in the carbon-containing species

TOF = (molar flow rates of reactants converted)/(moles of active nickel calculated from H_2 chemisorption)

Yield = (molar flow rates products produced)/(moles of active nickel calculated from H_2 chemisorption)

The carbon balance was within ±5% for all catalytic runs. Data for the catalyst activity were collected when the reaction reached stable conditions, and repeated tests have been run to confirm the activity.

It should be emphasized that according to the definitions, the sum of the selectivities of H_2 and the carbon-containing species does not lead to unity since they are calculated based on independent hydrogen and carbon balances, respectively.[30,31]

Results

Probe reaction analysis

Physicochemical properties of skeletal nickel-based catalysts and reference Ni/SiO_2 are shown in Table 1.[14] Skeletal Ni and Cu/skeletal Ni catalysts have comparable BET surface area, nickel size, and active nickel surface area, while the Ni/SiO_2 catalyst possesses larger nickel size and BET surface area compared to skeletal Ni-based catalysts.

The skeletal nickel-based catalysts show high reactivity in low-temperature steam reforming;[14] and there was no CO formed in the products. This was proposed to be due to the high activity in WGSR and methanation reactions of the catalyst.[32] Both probe reactions were therefore examined (Figures 1 and 2). From Figure 1, one can see that the skeletal nickel-based catalysts are more active on WGSR compared to the conventional supported Ni/SiO_2 catalyst, and the alloyed metal shows a promotional effect. CO conversion rate is higher on Cu/Ni, Co/Ni, Pt/Ni over the pure nickel catalyst. Since methane is the main hydrogen containing product, H_2 yield can be affected by the extent of the methanation reaction.[33] Experimental and theoretical investigations have demonstrated that CO dissociation on Ni is the rate-determining step for the methanation reaction.[34–37] CO adsorption ability of skeletal nickel catalyst is higher than that of Cu/Ni and Pt/Ni and lower than Co/Ni (Table 2).

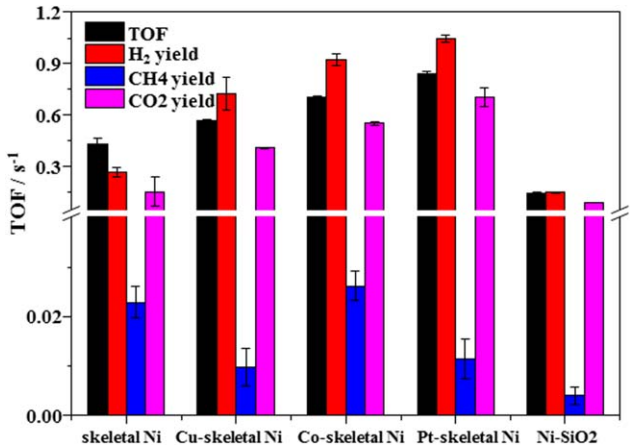

Figure 1. WGSR reactivity on skeletal nickel-based catalysts and the Ni/SiO_2 catalyst.

1 atm, 623 K; H_2O:CO:N_2 = 2:1:2; total flow rate: 100 mL/min. [Color figure can be viewed in the online issue, which is available at wileyonlinelibrary.com.]

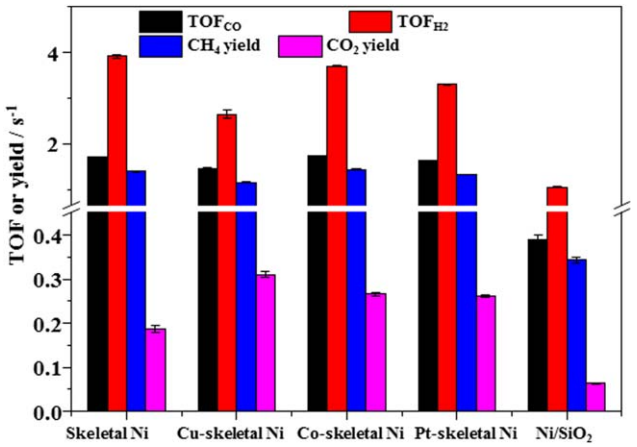

Figure 2. Methanation reactivity on skeletal nickel-based catalysts and the Ni/SiO_2 catalyst.

1 atm, 623 K; H_2:CO:N_2 = 3:1:1; total flow rate: 100 mL/min. [Color figure can be viewed in the online issue, which is available at wileyonlinelibrary.com.]

Therefore, we can rationalize that the presence of Cu and Pt could suppress the dissociation of CO on the Ni surface, and consequently suppress the methanation reaction, whereas Co could enhance the dissociation of CO on the Ni surface. Accordingly, the CO conversion rate on skeletal nickel and Co/Ni catalysts is higher compared to that on Cu/Ni and Pt/Ni, and CH_4 yield is higher on skeletal nickel and Co/Ni (Figure 2). Additionally, methanation reactivity of Ni/SiO_2 catalyst is much lower than that of skeletal nickel-based catalysts, which may be due to the higher nickel surface area that is typical considered as an active site for methane formation.

Accordingly, one can deduce that the higher activity of WGSR and methanation on skeletal nickel-based catalysts contributes to the elimination of CO in ESR. In order to elucidate the products distribution on skeletal nickel-based catalysts, skeletal nickel catalyst was chosen as a model to study the reaction scheme and kinetics of ESR. The effects of space-time, S/C, and temperature on products distribution were first examined. Figure 3a shows the effect of space-time on products distribution. At high-space times, only H_2, CO_2 and CH_4 are produced and no CO is formed. Upon reducing the space-time, CO is a primary product accompanied by the decrease of CO_2 and H_2 yield. These results

Table 2. CO Adsorption Properties of Skeletal Nickel-based Catalysts

Cat.	Skeletal Ni	Cu/Skeletal Ni	Co/Skeletal Ni	Pt/Skeletal Ni
CO/Ni atomic ratio	0.0055	0.0046	0.0057	0.0051

suggest that CO_2 could be formed by consecutive reaction (e.g., WGSR, as can be evidenced by the above probe reaction test). The yield of CH_4 decreases slightly with a declined space time, which can be due to the decreased reactivity of methanation reaction.

Figure 3b and 3c show the effect of S/C and temperature on ESR reactivity. It can be seen that H_2 and CO_2 yield increase with increasing S/C, while CO, CH_4 yield decrease with increasing S/C, which is due to the higher WGSR reactivity on increasing steam content (the order of water on WGSR is about 0.5).[38] Increasing water content can facilitate ethanol conversion and H_2 yield from thermodynamic point of view;[39] however, the promoting effect is not pronounced for the skeletal Ni on ethanol conversion, which is probably due to the low activity of Ni in dissociating water.[30] This indicates that water may take part in the reaction in molecular form. The effect of temperature on reactivity was further studied at high-space velocities (Figure 3c). One can see that ethanol conversion increases sharply with increasing temperature, which is due to the increasing reactivity of ethanol reforming. CO and CO_2 yields both increased slightly, implying that the WGSR reactivity is similar between 573 and 673 K. CH_4 yield decreases, implying the decreased reactivity of methanation. The overall effect of WGSR and methanation contributed to the increased H_2 yield. The thermodynamic composition was calculated for the studied conditions, the equilibrium H_2 yield is lower compared to experimental results (25% yield compared to 36% yield), which further prove the higher reactivity of skeletal nickel catalyst toward H_2 production.

Reaction scheme analysis

The reaction scheme of steam reforming of ethanol as a function of temperature was investigated employing TPRS experiments over skeletal Ni-based catalysts and Ni/SiO_2 catalyst. Figure 4a shows that ethanol desorption peaks appearing between 333 and 423 K. ED and dehydrogenation

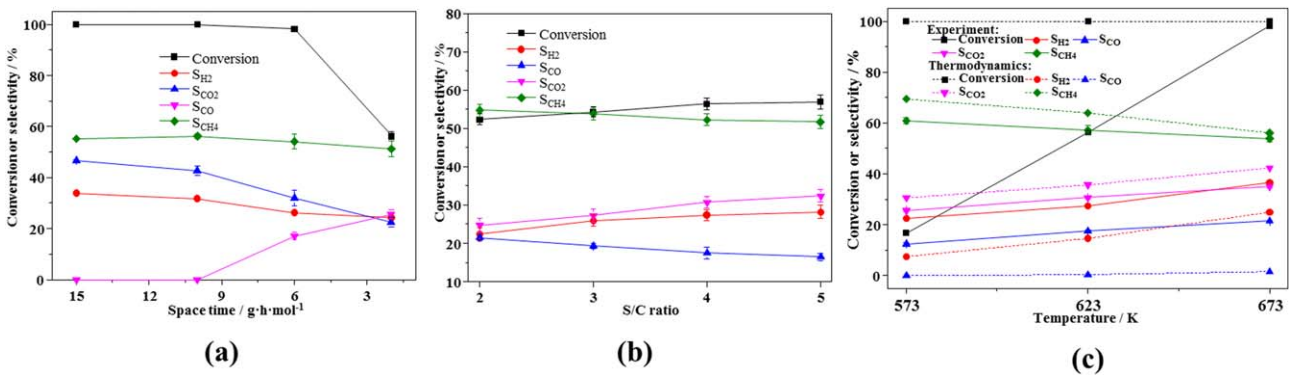

Figure 3. Effect of (a) space time (b) S/C, and (c) temperature on ESR reactivity over skeletal nickel.

Reaction conditions (a) 1 atm, 623 K, S/C = 4, ethanol in feed: 3.25%, (b) 1 atm, 623 K, W/F, 2 g·h/mol, ethanol in feed: 3.25%, and (c) 1 atm, S/C = 4, W/F = 2 g·h/mol, ethanol in feed: 3.25%. [Color figure can be viewed in the online issue, which is available at wileyonlinelibrary.com.]

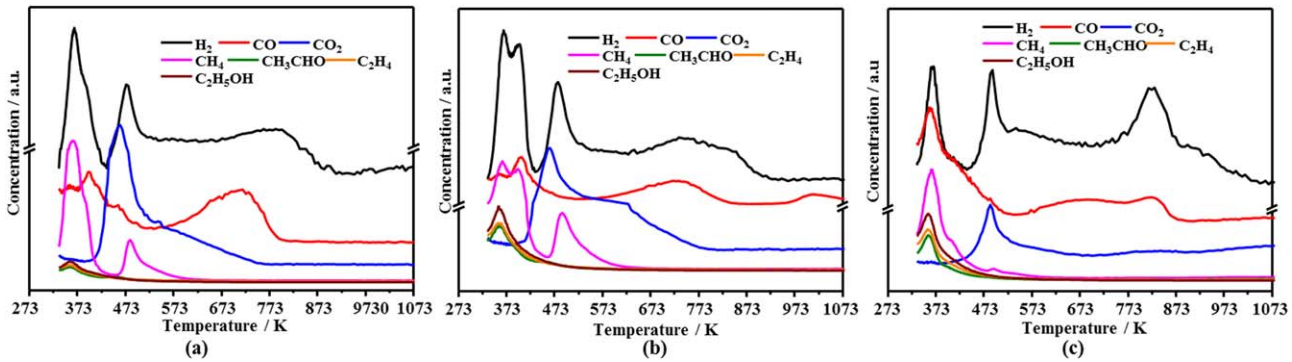

Figure 4. Temperature programmed reaction of ethanol on skeletal Ni, Cu/skeletal Ni, and Ni/SiO_2 catalysts.

[Color figure can be viewed in the online issue, which is available at wileyonlinelibrary.com.]

reactions (Eqs. 1 and 2)[6] are initiated in the same temperature range producing H_2, CO, CH_4 and CH_3CHO. The concentration peaks of CO and CH_4 are similar, as expected from Eq. 1, in contrast to H_2 concentration which is significantly higher probably due to the occurrence of dehydrogenation of ethanol (Eq. 2). The decrease in the concentration of CO was observed at 423–623 K, which is accompanied by increased concentrations of CO_2 and H_2 concentration, attributed to the WGSR[40] (Eq. 3). However, the difference in the concentrations of H_2 and CO_2 and the evolution of CH_4 peak evidence that the methanation also took place at this temperature range[41] (Eq. 4). In the temperature range of 623–873 K, the increase of H_2 and CO concentrations, in association with the lowest CO_2 and CH_4 concentrations, indicate that MSR (Eq. 4) is the main reaction, which is completed at about 873 K

$$C_2H_5OH \rightarrow CO + CH_4 + H_2 \quad (1)$$

$$C_2H_5OH \rightarrow CH_3CHO + H_2 \quad (2)$$

$$CO + H_2O \leftrightarrow CO_2 + H_2 \quad (3)$$

$$CH_4 + H_2O \leftrightarrow CO + 3H_2 \quad (4)$$

$$C_2H_5OH \rightarrow C_2H_4 + H_2O \quad (5)$$

The ethanol desorption on Cu/skeletal nickel is similar with that of skeletal nickel except for desorption temperatures of H_2 and CO_2, which could be due to the different adsorption ability on copper and nickel.[42] On the Ni/SiO_2 catalyst, a higher desorption peak of C_2H_4 and CH_3CHO appears in the 333–423 K range, which is due to ethanol dehydrogenation (Eq. 2) and dehydration (Eq. 5) reactions. Additionally, there is no methane desorption peak observed in the 423–623 K range, indicating the lower methanation reactivity on the Ni/SiO_2 catalyst. However, the H_2 desorption peak in 623–873 K range is higher compared to that on skeletal nickel-based catalysts, implying the higher reactivity of MSR on supported nickel catalysts at high temperatures.

There are no significant differences between TPRS of ethanol-steam (Figure 5) and ethanol desorption on various skeletal nickel-based catalysts. However, different patterns were observed on Ni/SiO_2; weak CO concentration was detected in 623–873 K range. This could be owing to the dissociation of water on the oxide surface[43] (Eq. 6) and the enhanced reaction of adsorbed hydroxyls with CO. Kim et al.[44] have reported that the hydroxyl groups (—OH) present on the silica surface could result in high selectivity toward the WGSR than to methanation

$$H_2O \xleftarrow[\text{dissociatively adsorption}]{\text{supported catalysts}} [H] + [OH] \quad (6)$$

In order to further study the instantaneous reaction pathway at different temperature range, we have carried out the transient experiments at a steady state (denoted as the temperature programmed surface reactions). The surface reactions over various catalysts were investigated as a function of temperature, employing transient experiments in which temperature was ramped linearly from 323 to 1073 K at a rate of 10 K/min while an ethanol-steam mixture was flowing at a steady rate over the catalyst. Figure 6 shows that there is no difference between skeletal nickel and Cu/Ni. There are mainly three H_2 concentration peaks (e.g., three reactions producing H_2) observed, and C2 products and/or intermediates were all converted. The first H_2 concentration peak in the 333–423 K range can be ascribed to ED;[6] CO and CH_4 concentration peaks were also observed in this temperature range. The second concentration peak is accompanied by CH_4 and CO_2 in the 423–623 K range, indicating the high activity of methanation and WGSR about 523 K. The third peak could be attributed to ED and MSR; since water is highly consumed at this temperature range, WGSR reactivity is inhibited.[45] The transient reaction results on Ni/SiO_2 catalyst were similar with that on skeletal nickel-based catalysts, except that ethanol and C2 products were not fully converted at the first concentration peak range implying that skeletal nickel-based catalysts are more active in C—C bond cleavage. The second concentration peak (methanation and WGSR) appears at ~573 K (50 K higher than that of skeletal nickel-based catalysts). This result suggests that skeletal nickel-based catalysts are more active compared to conventional Ni/SiO_2 catalyst due to the larger active nickel surface area.[46] In the 623–873 K range, H_2, CO, and H_2O concentration peaks are similar between skeletal nickel-based catalysts and Ni/SiO_2 catalyst, implying the comparable MSR and ESR reactivity at high temperatures.

Accordingly, we can obtain a preliminary reaction pathway of ESR on nickel based catalysts (as shown in Scheme 1). Ethanol first dehydrogenates to CH_3CHO on nickel, since the bond breaking sequence on pure nickel follows the following order: O—H, —CH_2—, C—C, and —CH_3.[8,9] While when there is acidic support, ethanol also dehydrates to C_2H_4. Nickel has high ability in C—C bond cleavage, so the formed CH_3CHO would fast decompose into CH_4 and CO,[6] which can also be

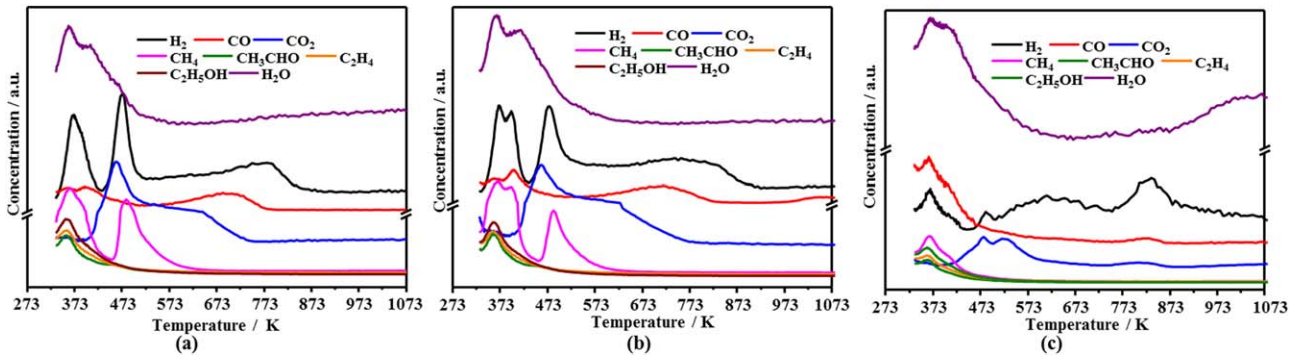

Figure 5. Temperature programmed reaction of ethanol-steam on (a) skeletal Ni, (b) Cu/skeletal Ni, and (c) Ni/SiO_2 catalysts.

[Color figure can be viewed in the online issue, which is available at wileyonlinelibrary.com.]

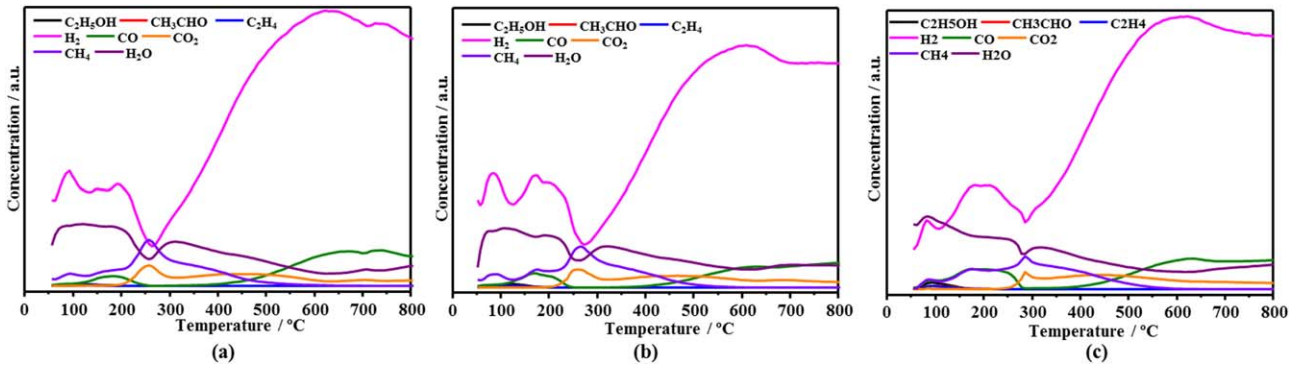

Figure 6. Temperature-programmed surface reaction of EtOH and H_2O on (a) skeletal Ni, (b) Cu/skeletal Ni, and (c) Ni/SiO_2 catalysts.

[Color figure can be viewed in the online issue, which is available at wileyonlinelibrary.com.]

proved by the low signal of CH_3CHO in temperature programmed transient reactions. The formed CH_4 would be reformed to CO and H_2 in the presence of steam, and CO will be transformed into CO_2 through WGSR.[47] Water will be dissociated with the help of support,[30,48] otherwise it participates in the reaction in molecular form (without dissociation) (e.g., skeletal nickel catalyst).

Kinetic model

The following hypotheses are assumed to narrow the wide variety of possible models.

1. All species are adsorbed on the same type of active site. As demonstrated in previous investigations for nickel-based catalysts under similar conditions,[16,22] ethanol, CO and methane adsorb and react on the same type of active site.

2. The existence of a controlling step in the reaction is assumed. This allows solving the system using the RDS method.

3. From TPRS experiments and product distributions at different reaction conditions, coke deposition rate was slow,[14] and formation of C_2H_4 and CH_3CHO was nearly negligible. Therefore, the production of C_2H_4 and CH_3CHO

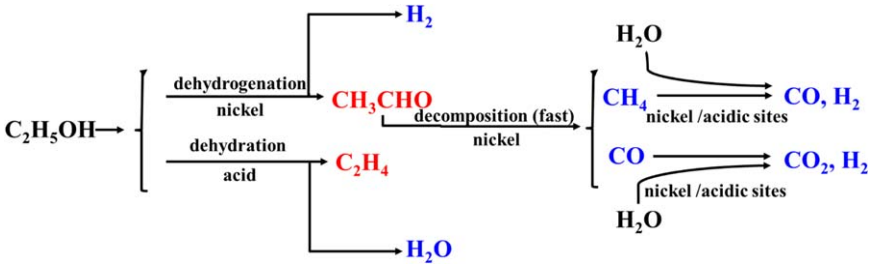

Scheme 1. Reaction scheme of ESR on nickel based catalysts.

[Color figure can be viewed in the online issue, which is available at wileyonlinelibrary.com.]

Table 3. Quotient (the Equilibrium Constant (K) Divided by the Ratios of Partial Pressures (Q_p)) of MSR and WGSR at ESR Conditions in Figure 5

	573 K	623 K	673 K
WGSR	0.0018	0.0039	0.222
MSR	0.00012	0.0065	0.0069

$Q_p(WGSR)=\frac{P_{CO_2}\bullet P_{H_2}}{P_{CO}\bullet P_{H_2O}}$.

$Q_p(MSR)=\frac{(P_{H_2})^3\bullet P_{CO}}{P_{CH_4}\bullet P_{H_2O}}$.

and the reactions involving the formation and/or consumption of coke are discarded in our kinetic model.

4. As described earlier, dissociative probability of water adsorption on skeletal nickel catalyst is fairly low, so we assume that water takes part in reaction in molecular form. Thus, the E-R mechanism is proposed for the kinetic study.

Based on the information available in the literature and our obtained experimental results, the model can be expressed as follows

$$C_2H_5OH+* \overset{k_1}{\leftrightarrow} C_2H_5OH* \quad (7)$$

$$C_2H_5OH* \rightarrow CH_3CHO*+H_2 \quad (8)$$

$$CH_3CHO*+* \overset{k_2}{\longrightarrow} CH_4*+CO* \quad (9)$$

$$CH_4*+H_2O \overset{k_3}{\leftrightarrow} CO*+3H_2 \quad (10)$$

$$CO*+H_2O \overset{k_4}{\leftrightarrow} CO_2*+H_2 \quad (11)$$

$$CO* \overset{k_5}{\leftrightarrow} CO+* \quad (12)$$

$$CO_2* \overset{k_6}{\leftrightarrow} CO_2+* \quad (13)$$

$$CH_4* \overset{k_7}{\leftrightarrow} CH_4+* \quad (14)$$

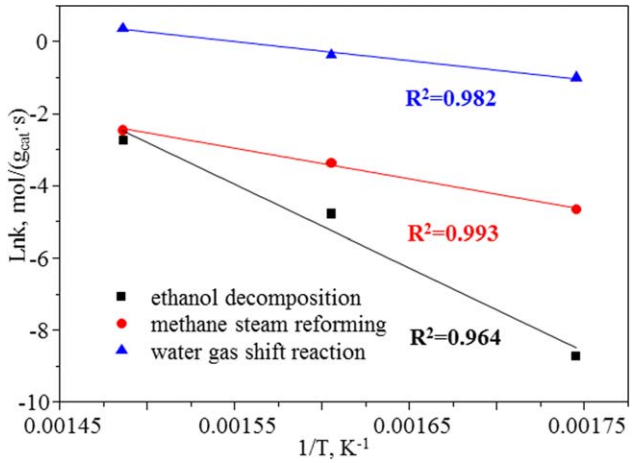

Figure 8. Arrhenius plot of rate coefficients for the kinetic model.

[Color figure can be viewed in the online issue, which is available at wileyonlinelibrary.com.]

It has been reported that the possible controlling steps are C—C rupture[15] and surface reactions (e.g., ESR, ED, WGSR, and MSR).[17,19,21] If the former is the controlling step, the MSR and WGSR would be in equilibrium.[16] According to a previous investigation by the Dumesic group,[49] the quotient (Q_p/K) is used to judge if a reaction is in equilibrium (e.g., if the quotient equals 1, the reaction is in equilibrium). However, Table 3 indicates that both reactions are far from equilibrium. Therefore, in our model surface reactions (ED (reactions 8 and 9), MSR (reaction 9), and WGSR (reaction 10) were first considered as not in equilibrium. Since CH_3CHO is not detected in the products, reaction 9 was very

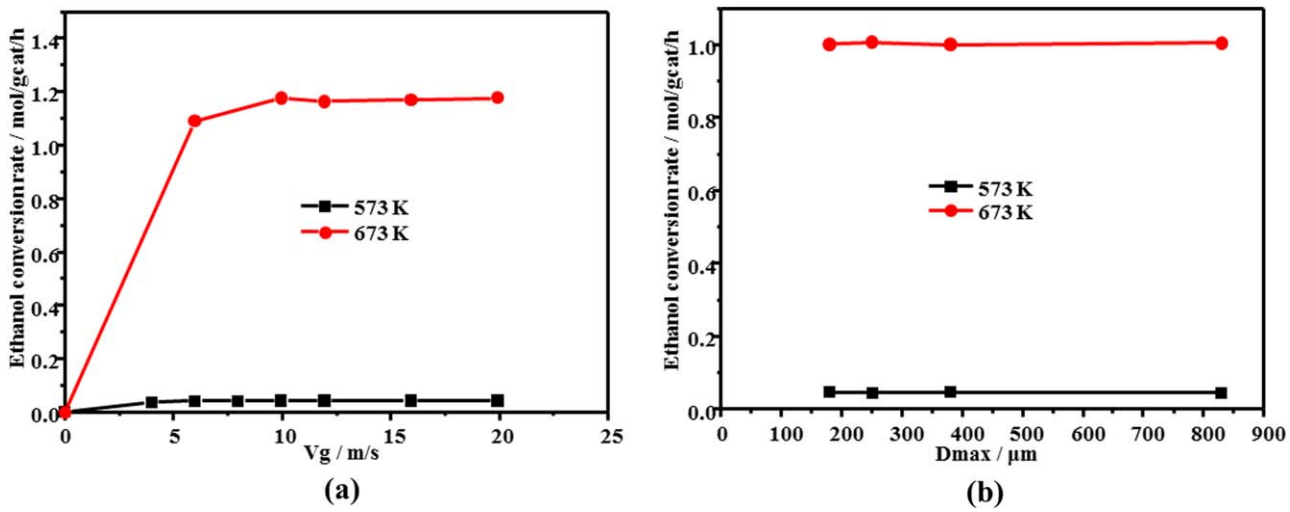

Figure 7. Ethanol conversion rate on skeletal nickel catalyst as a function of (a) gas velocity, and (b) particle size at 300 and 400°C.

Reaction conditions: P = 1 atm, ethanol in feed: 3.25%, S/C = 4, and W/F = 2 g·h/mol. [Color figure can be viewed in the online issue, which is available at wileyonlinelibrary.com.]

Table 4. Constants of Reaction Rate and Adsorption Balance under Different Temperature

Temperature/K	k_2/(mol/g/h)	k_3/(mol/g/h)	k_4/(mol/g/h)	K_{et}/atm^{-1}	K_{CO}/atm^{-1}	K_{CO2}/atm^{-1}	K_{CH4}/atm^{-1}
673	0.063	0.76	1.95	9.75	3.74	38.09	7.41
623	0.00085	0.035	0.69	17.70	158.62	194.73	15.89
573	0.00017	0.0096	0.37	31.17	561.59	1947.30	129.90

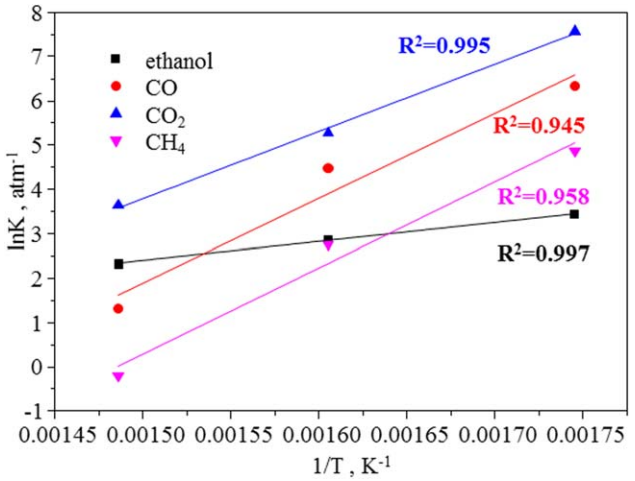

Figure 9. Van't Hoff plot of adsorption coefficients for the kinetic model.

[Color figure can be viewed in the online issue, which is available at wileyonlinelibrary.com.]

Table 5. Activation Energy and Index Factor of ESR

Reaction	ED	MSR	WGSR
Activation energy/kJ/mol	187.7±5.8	138.5±3.9	52.8±1.0
Index factor/(mol/g-cat./h)	$1.32*10^{13}$	$2.90*10^{10}$	$2.20*10^{5}$

Table 6. Adsorption Enthalpy of the Reactants

Reactants	Ethanol	CO	CO_2	CH_4
Adsorption enthalpy/(kJ/mol)	−37.2	−158.0	−126.4	−92.8

fast, and reactions 8 and 9 were combined in calculation for simplicity. Solving the system we obtain

$$r_{ED} = k_2 K_1 P_{et} C_v^2 \tag{15}$$

$$r_{SRM} = k_3 \left(\frac{P_{CH_4} P_{H_2O}}{K_7} - \frac{P_{CO} P_{H_2}^3}{K_3 K_5} \right) C_v \tag{16}$$

$$r_{WGS} = k_4 \left(\frac{P_{CO} P_{H_2O}}{K_5} - \frac{P_{CO_2} P_{H_2}}{K_4 K_6} \right) C_v \tag{17}$$

$$C_v = \frac{1}{1 + K_1 P_{et} + P_{CO}/K_5 + P_{CO_2}/K_6 + P_{CH_4}/K_7} \tag{18}$$

$$k_i = k_{0,i} \exp\left(-\frac{E_{a,i}}{RT} \right) \tag{19}$$

$$K_i = K_{i0} \exp\left(-\frac{\Delta H_{fi}}{RT} \right) \tag{20}$$

We eliminate internal and external diffusional resistance to ensure that experimental results used for kinetic analysis falling into reaction control zone. Preliminary ESR runs were carried out with different catalyst particle size and with different gas space velocity. The effect of gas velocity on ethanol conversion rate was evaluated varying the volumetric flow rate from 200 to 1000 mL/min at 573 and 673 K (Figure 7a). Since the ethanol conversion rate is almost constant in the gas velocity above 10 m/s for the temperatures examined, a volumetric flow rate of 600 mL/min has been used for all the kinetic runs in order to eliminate the external diffusional resistance.

The effect of catalyst particle size was also evaluated varying the particle size from 150 to 850 μm at 573 and 673 K (Figure 7b). Ethanol conversion rate is almost constant for a particle size diameter ranging from 150 to 400 μm, indicating that the reaction rate is not limited by internal diffusion resistance in this range of diameter values. Moreover, in order to eliminate channeling effects, the following conditions must be satisfied

$$(L_r/d_p) > 50$$

$$(d/d_p) > 10$$

L_r refers to the length of catalyst bed, d refers to the inner diameter of the flow reactor, and d_p refers to the particle size of catalyst. Therefore, we selected a particle diameter range of 60–80 mesh for the catalytic runs.

Parameter estimation

Kinetic runs were carried out by varying the S/C or temperature, keeping constant the other operating conditions, and measuring the rates of ethanol conversion and of H_2, CO, CO_2, and CH_4 yield. A randomized algorithms method was used to solve the differential equations (Eqs. 15–18), and the experimental data were fitted by a least-squares method. The obtained kinetic values are listed in Table 4; according to Eqs. 19, 20, the rate and adsorption coefficients of the Arrhenius plot and Van't Hoff plot are shown in Figures 8 and 9. Activation energy and adsorption enthalpy can then be derived from the slopes of the Arrhenius plot and Van't Hoff plot as listed in Tables 5 and 6. Table 5 shows that ED should be rate determining reaction of ESR on skeletal nickel catalyst with the highest activation energy. The activation energy of WGSR is much lower than that of ED and MSR, which may account for the particularly low CO level observed on this catalyst.

The goodness of fit obtained with this model is above 0.95. The estimated values for this model are consistent with those reported previously[16,17,19,21,50] as shown in Table 7. The kinetic model was further examined by estimating the flow rate of products using the kinetic expressions and parameters obtained in this work. Experimental measured flow rate of products vs. the values calculated using the

Table 7. Activation Energy Values Reported in the Literature

				Activation Energy [kJ/mol]		
Reference	T [K]	Catalyst	Kinetics	ED	MSR	WGS
This work	573–623	Skeletal nickel	ER	187.7	138.5	52.8
Llera *et al.*[16]	873–923	Ni-Al-O	LHHW	122.9	174.0	166.3
Graschinsky *et al.*[17]	773–873	$Rh(1\%)MgAl_2O_4/Al_2O_3$	LHHW	85.9	151	107
Mas *et al.*[19]	823–923	Ni-Al-O	ER	278.7	123.5	—
Vaidya *et al.*[50]	873–973	Ru/γ-Al_2O_3	Power law	96	—	—
Sahoo *et al.*[21]	673–973	Co/Al_2O_3	LHHW	71.3	—	43.6

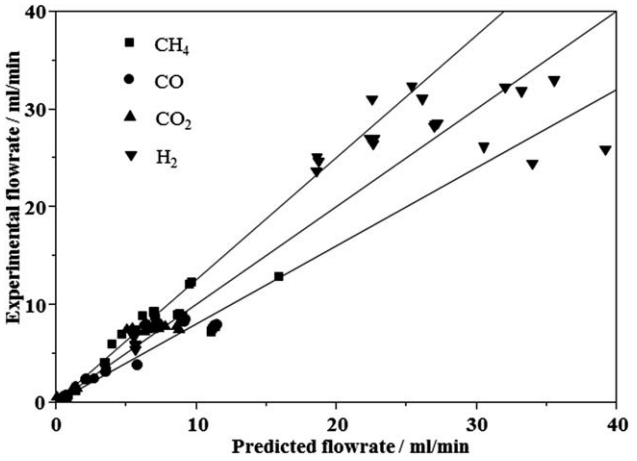

Figure 10. Parity plots for the various flow rates of products.

retained model is shown in Figure 10. One can see that the estimation error for each flow rate is within 10%, which can be appreciated that the fit is satisfactory. This could be a criterion that strengthens our proposed kinetic model.

Conclusions

The low-temperature reactivity of ESR on skeletal nickel catalyst is detailed at 573–673 K. The catalysts are very active and selective for the production of H_2 at low temperatures, allowing high-ethanol conversion with very low selectivity to CO. Moreover, Cu and Pt addition can promote WGSR and MSR, and thus further improve H_2 production. The reasons for the low CO level were also attained by probe reactions. A series of TPRS experiments were carried out to obtain the reaction pathway of ESR. Moreover, we have first proposed a mechanism of ESR on pure nickel catalyst, which includes ED, WGSR, and MSR reactions. An E-R mechanism was used for the kinetic study, a randomized algorithms method and a least-squares method to solve the differential equations and fit the experimental data, and the goodness of fit obtained with this model is above 0.95. The activation energies of the ED, MSR, WGSR reactions are estimated to be 187.7 kJ/mol, 138.5 kJ/mol and 52.8 kJ/mol, respectively. Thus, ED was the rate determining reaction of ESR on skeletal nickel catalyst. It should be noted that this kinetic study is only useful for skeletal nickel or unsupported nickel catalysts.

Acknowledgments

This work is supported by the National Science Foundation of China (21006068, 21222604, 21206115), the Program for New Century Excellent Talents in University (NCET-10-0611), Specialized Research Fund for the Doctoral Program of Higher Education (20120032110024), the Scientific Research Foundation for the Returned Overseas Chinese Scholars (MoE), Seed Foundation of Tianjin University (60303002), and the Program of Introducing Talents of Discipline to Universities (B06006).

Literature Cited

1. Chheda JN, Huber GW, Dumesic JA. Liquid-phase catalytic processing of biomass-derived oxygenated hydrocarbons to fuels and chemicals. *Angew Chem Int Ed.* 2007;46(38):7164–7183.
2. James OO, Maity S, Mesubi MA, et al. Towards reforming technologies for production of hydrogen exclusively from renewable resources. *Green Chem.* 2011;13(9):2272–2284.
3. Haryanto A, Fernando S, Murali N, Adhikari S. Current status of hydrogen production techniques by steam reforming of ethanol: A review. *Energ Fuel.* 2005;19(5):2098–2106.
4. Holladay J, Hu J, King D, Wang Y. An overview of hydrogen production technologies. *Catal Today.* 2009;139(4):244–260.
5. Ni M, Leung DYC, Leung MKH. A review on reforming bio-ethanol for hydrogen production. *Int J Hydrogen Energ.* 2007; 32(15):3238–3247.
6. Fatsikostas AN, Verykios XE. Reaction network of steam reforming of ethanol over Ni-based catalysts. *J Catal.* 2004;225(2):439–452.
7. Comas J, Mariño F, Laborde M, Amadeo N. Bio-ethanol steam reforming on Ni/Al_2O_3 catalyst. *Chem Eng J.* 2004;98(1-2):61–68.
8. Gates SM, Russell Jr JN, Yates Jr JT. Bond activation sequence observed in the chemisorption and surface reaction of ethanol on Ni(111). *Surf Sci.* 1986;171(1):111–134.
9. Xu J, Zhang X, Zenobi R, Yoshinobu J, Xu Z, Yates Jr JT. Ethanol decomposition on Ni(111): observation of ethoxy formation by IRAS and other methods. *Surf Sci.* 1991;256(3):288–300.
10. Wu G, Zhang C, Li S, et al. Sorption enhanced steam reforming of ethanol on $Ni\text{-}CaO\text{-}Al_2O_3$ multifunctional catalysts derived from hydrotalcite-like compounds. *Energ Environ Sci.* 2012;5:8765–9136.
11. Li S, Zhang C, Huang Z, Wu G, Gong J. A $Ni@ZrO_2$ nanocomposite for ethanol steam reforming: enhanced stability via strong metal-oxide interaction. *Chem Commun.* 2013;49(39):4226–4228.
12. Zhou G, Barrio L, Agnoli S, et al. High Activity of $Ce_{1-x}Ni_xO_{2-y}$ for H_2 Production through ethanol steam reforming: tuning catalytic performance through metal-oxide interactions. *Angew Chem Int Ed.* 2010;49(50):9680–9684.
13. Hu X, Lu GX. Inhibition of methane formation in steam reforming reactions through modification of Ni catalyst and the reactants. *Green Chem.* 2009;11(5):724–732.
14. Zhang C, Zhang P, Li S, Wu G, Ma X, Gong J. Superior reactivity of skeletal Ni-based catalysts for low-temperature steam reforming to produce CO-free hydrogen. *Phys Chem Chem Phys.* 2012;14(10):3295–3298.
15. Akande A, Aboudheir A, Idem R, Dalai A. Kinetic modeling of hydrogen production by the catalytic reforming of crude ethanol over a co-precipitated $Ni\text{-}Al_2O_3$ catalyst in a packed bed tubular reactor. *Int J Hydrogen Energ.* 2006;31(12):1707–1715.
16. Llera I, Mas V, Bergamini ML, Laborde M, Amadeo N. Bio-ethanol steam reforming on Ni based catalyst. *Kinetic study. Chem Eng Sci.* 2012;71:356–366.
17. Graschinsky C, Laborde M, Amadeo N, et al. Ethanol steam reforming over $Rh(1\%)MgAl_2O_4/Al_2O_3$: A kinetic Study. *Ind Eng Chem Res.* 2010;49(24):12383–12389.
18. Ciambelli P, Palma V, Ruggiero A. Low temperature catalytic steam reforming of ethanol. 2. Preliminary kinetic investigation of Pt/CeO_2 catalysts. *Appl Catal B.* 2010;96(1-2):190–197.
19. Mas V, Bergamini ML, Baronetti G, Amadeo N, Laborde M. A kinetic study of ethanol steam reforming using a nickel based catalyst. *Top Catal.* 2008;51(1-4):39–48.
20. Peela NR, Kunzru D. Steam reforming of ethanol in a microchannel reactor: kinetic study and reactor simulation. *Ind Eng Chem Res.* 2011;50(23):12881–12894.
21. Sahoo DR, Vajpai S, Patel S, Pant KK. Kinetic modeling of steam reforming of ethanol for the production of hydrogen over Co/Al_2O_3 catalyst. *Chem Eng J.* 2007;125(3):139–147.
22. Akpan E, Akande A, Aboudheir A, Ibrahim H, Idem R. Experimental, kinetic and 2-D reactor modeling for simulation of the production of hydrogen by the catalytic reforming of concentrated crude ethanol (CRCCE) over a Ni-based commercial catalyst in a packed-bed tubular reactor. *Chem Eng Sci.* 2007;62(12):3112–3126.
23. Wang J-H, Lee CS, Lin MC. Mechanism of ethanol reforming: Theoretical foundations. *J Phys Chem C.* 2009;113(16):6681–6688.
24. Fatsikostas A. Reaction network of steam reforming of ethanol over Ni-based catalysts. *J Catal.* 2004;225(2):439–452.
25. Busca G, Montanari T, Resini C, Ramis G, Costantino U. Hydrogen from alcohols: IR and flow reactor studies. *Catal Today.* 2009;143(1-2):2–8.
26. Resini C, Montanari T, Barattini L, et al. Hydrogen production by ethanol steam reforming over Ni catalysts derived from hydrotalcite-like precursors: Catalyst characterization, catalytic activity and reaction path. *Appl Catal A.* 2009;355(1-2):83–93.
27. Mariño F, Boveri M, Baronetti G, Laborde M. Hydrogen production via catalytic gasification of ethanol. *A mechanism proposal over copper-nickel catalysts. Int J Hydrogen Energ.* 2004;29(1):67–71.

28. Raskó J, Hancz A, Erdőhelyi A. Surface species and gas phase products in steam reforming of ethanol on TiO_2 and Rh/TiO_2. *Appl Catal A*. 2004;269(1-2):13–25.
29. Dömök M, Tóth M, Raskó J, Erdőhelyi A. Adsorption and reactions of ethanol and ethanol-water mixture on alumina-supported Pt catalysts. *Appl Catal B*. 2007;69(3-4):262–272.
30. Zhu LJ, Guo PJ, Chu XW, et al. An environmentally benign and catalytically efficient non-pyrophoric Ni catalyst for aqueous-phase reforming of ethylene glycol. *Green Chem*. 2008;10(12):1323–1330.
31. Song H, Mirkelamoglu B, Ozkan US. Effect of cobalt precursor on the performance of ceria-supported cobalt catalysts for ethanol steam reforming. *Appl Catal A*. 2010;382(1):58–64.
32. Chen L, Choong CKS, Zhong Z, et al. Carbon monoxide-free hydrogen production via low-temperature steam reforming of ethanol over iron-promoted Rh catalyst. *J Catal*. 2010;276(2):197–200.
33. Li S, Li M, Zhang C, Wang S, Ma X, Gong J. Steam reforming of ethanol over Ni/ZrO_2 catalysts: Effect of support on product distribution. *Int J Hydrogen Energ*. 2012;37(3):2940–2949.
34. Goodwan DW, Kelley RD, Madey TE, White JM. Measurement of carbide buildup and removal kinetics on Ni(100). *J Catal*. 1980; 64(2):479–481.
35. Bell AT. Catalytic synthesis of hydrocarbons over Group VIII metals. *Discussion of the reaction mechanism. Catal Rev Sci Eng*. 1981; 23(1-2):203–232.
36. Coenen JWE, van Nisselrooy PFMT, de Croon MHJM, van Dooren PFHA, van Meerten RZC. The dynamics of methanation of carbon monoxide on nickel catalysts. *Appl Catal*. 1986;25(C):1–8.
37. Sehested J, Dahl S, Jacobsen J, Rostrup-Nielsen JR. Methanation of CO over nickel: Mechanism and kinetics at high H_2/CO ratios. *J Phys Chem. B*. 2005;109(6):2432–2438.
38. Grabow LC, Gokhale AA, Evans ST, Dumesic JA, Mavrikakis M. Mechanism of the water gas shift reaction on Pt: First principles, experiments, and microkinetic modeling. *J Phys Chem C*. 2008; 112(12):4608–4617.
39. Mas V, Kipreos R, Amadeo N, Laborde M. Thermodynamic analysis of ethanol/water system with the stoichiometric method. *Int J Hydrogen Energ*. 2006;31(1):21–28.
40. Benito M, Padilla R, Serrano-Lotina A, Rodriguez L, Brey JJ, Daza L. The role of surface reactions on the active and selective catalyst design for bioethanol steam reforming. *J Power Sources*. 2009; 192(1):158–164.
41. Padilla R, Benito M, Rodríguez L, Serrano A, Muñoz G, Daza L. Nickel and cobalt as active phase on supported zirconia catalysts for bio-ethanol reforming: Influence of the reaction mechanism on catalysts performance. *Int J Hydrogen Energy*. 2010;35(17):8921–8928.
42. Wang JH, Lee CS, Lin MC. Mechanism of ethanol reforming: Theoretical foundations. *J Phys Chem C*. 2009;113(16):6681–6688.
43. Kim YD, Wei T, Stultz J, Goodman DW. Dissociation of water on a flat, ordered silica surface. *Langmuir*. 2003;19(4):1140–1142.
44. Kim SH, Chung JH, Kim YT, et al. SiO_2/Ni and CeO_2/Ni catalysts for single-stage water gas shift reaction. *Int J Hydrogen Energ*. 2010;35(7):3136–3140.
45. Sanchez-Sanchez MC, Yerga RMN, Kondarides DI, Verykios XE, Fierro JLG. Mechanistic aspects of the ethanol steam reforming reaction for hydrogen production on pt, ni, and ptni catalysts supported on gamma-Al2O3. *J Phys Chem A*. 2010;114(11):3873–3882.
46. Huber GW. Raney Ni-Sn catalyst for H_2 production from biomass-derived hydrocarbons. *Science*. 2003;300(5628):2075–2077.
47. Li S, Zhang C, Zhang P, Wu G, Ma X, Gong J. On the origin of reactivity of steam reforming of ethylene glycol on supported Ni catalysts. *Phys Chem Chem Phys*. 2012;14(12):4066–4069.
48. Grenoble DC, Estadt MM, Ollis DF. The chemistry and catalysis of the water gas shift reaction: 1. *The kinetics over supported metal catalysts*. *J Catal*. 1981;67(1):90–102.
49. Shabaker JW, Davda RR, Huber GW, Cortright RD, Dumesic JA. Aqueous-phase reforming of methanol and ethylene glycol over alumina-supported platinum catalysts. *J Catal*. 2003;215(2):344–352.
50. Vaidya PD, Rodrigues AE. Kinetics of steam reforming of ethanol over a Ru/Al_2O_3 catalyst. *Ind Eng Chem Res*. 2006;45(19):6614–6618.

Manuscript received Jun. 12, 2013, and revision received Aug. 13, 2013.